Available online at www.sciencedirect.com
SCIENCE DIRECT®
Microporous and Mesoporous Materials 65 (2003) 177–187
MICROPOROUS AND MESOPOROUS MATERIALS
www.elsevier.com/locate/micromeso

The influence of aluminium sources on the acidic behaviour as well as on the catalytic activity of mesoporous H-AlMCM-41 molecular sieves

A. Sakthivel [a], S.E. Dapurkar [a], N.M. Gupta [b], S.K. Kulshreshtha [c], P. Selvam [a,*]

[a] *Department of Chemistry, Indian Institute of Technology-Bombay, Powai, Mumbai 400 076, India*
[b] *Applied Chemistry Division, Bhabha Atomic Research Centre, Trombay, Mumbai 400 085, India*
[c] *Novel Materials and Structural Chemistry Division, Bhabha Atomic Research Centre, Trombay, Mumbai 400 085, India*

Received 2 April 2003; received in revised form 22 July 2003; accepted 22 August 2003

Abstract

A series of mesoporous molecular sieves (AlMCM-41) were synthesized with varying silicon-to-aluminium ratios and using three different aluminium sources, viz., sodium aluminate, aluminium isopropoxide and aluminium sulphate. The samples were characterized systematically using XRD, TG-DTA, BET surface area, and ICP-AES. In addition, the extent of framework substitution as well as the nature of acid sites was deduced employing ^{27}Al MAS-NMR, pyridine FT-IR, and NH_3-TPD methods. These studies indicate that in case of samples prepared with sodium aluminate, most of the aluminium existed in tetrahedral positions even after calcination. Also, such samples posses moderate-to-strong (Brönsted) acid sites along with small amounts of structural as well as non-framework Lewis acid sites. The density of non-framework acid sites depended upon the source of aluminium following a trend in the order of sodium aluminate < aluminium sulphate < aluminium isopropoxide. Among the various catalysts investigated, those having a silicon-to-aluminium ratio of around 60 irrespective of aluminum sources exhibited highest conversion and good selectivity for vapour phase *tertiary*-butylation of phenol. This characteristic is attributed to the presence of larger number of moderate-to-strong acid sites and a smaller number of Lewis acid sites.

Keywords: Mesoporous materials; Aluminium sources; Butylation of phenol; AlMCM-41

1. Introduction

The identification and development of new heterogeneous solid acid catalysts for fine chemical and petrochemical products is becoming an area of growing interest [1,2]. In this regard, the discovery of mesoporous materials, designated as MCM-41 and MCM-48 having regular pore size and large surface area have opened new possibilities in the field of adsorption and heterogeneous catalysis [3,4]. It has been reported that the isomorphous substitution of trivalent aluminium into the silicate framework (e.g., AlMCM-41) show promise for several organic reactions [5–7]. It is, however, important to note that the incorporation of

* Corresponding author. Tel.: +91-22-2576-7155; fax: +91-22-2572-3480/2576-7152.
E-mail address: selvam@iitb.ac.in (P. Selvam).

1387-1811/$ - see front matter © 2003 Elsevier Inc. All rights reserved.
doi:10.1016/j.micromeso.2003.08.004

aluminium in the tetrahedral framework depends strongly on the source of aluminium used for the preparation [8–17]. For example, Janicke et al. [8], and Reddy and Song [11] have claimed aluminium isopropoxide as a better source as compared to aluminium sulphate and pseudobohmite. While Luan et al. [10] have favoured aluminium sulphate among the other aluminium sources like catapal alumina (75% Al_2O_3; Vista Chemicals), aluminium orthophosphate, aluminium acetylacetonate, aluminium isopropoxide and aluminium hydroxide-hydrate. On the contrary, Borade and Clearfiled [9] Occelli et al. [14] and Badamali et al. [16] have reported sodium aluminate source incorporates aluminium to a maximum amount in the framework sites. In addition, density and the strength of acid sites are found to be significantly higher using sodium aluminate as compared to aluminium isopropoxide or aluminium hydroxide [14]. However, less attention has been focused on the effect of varying aluminium sources and silicon-to-aluminium ratios on the acid site distribution as well as catalytic properties.

On the other hand, *tertiary*-butylation reaction products of phenol, e.g., *para-tertiary*-butyl phenol (*p-t*-BP) and 2,4-di-*tertiary*-butyl phenol (2,4-di-*t*-BP), are widely used in the manufacture of phenolic resins, antioxidants and polymerization inhibitors [1]. Numerous reports on the production of these alkyl-substituted phenols over various heterogeneous solid acid catalysts are available in literature [18–33]. However, the substrate conversion as well as selectivity are found to depend mainly on the acidic characteristics of the materials [30]. For example, while the weak acidic catalyst such as partially Na^+- or K^+-exchanged zeolite-Y leads to oxygen-alkylated product (*tertiary*-butyl phenyl ether; *t*-BPE) [23], strong acidic catalyst, e.g., zeolite-β [28] produces carbon-alkylated product (*meta-tertiary*-butyl phenol; *m-t*-BP), which is formed by the isomerization of initially formed *ortho-tertiary*-butyl phenol (*o-t*-BP) and *para-tertiary*-butyl phenol (*p-t*-BP). On the other hand, moderate acidic catalysts such as zeolite-Y [23], ZSM-12 [24] and SAPO-11 [27] are found to be suitable for the formation of *p*-isomer.

Realizing the importance of the solid acid catalysts as well as the prevailing discrepancy over framework substitution of aluminium in MCM-41 using various aluminium sources, in the present investigation a systematic study have been carried out on the incorporation of trivalent aluminium in MCM-41 using the best claimed aluminium sources, by various groups, [8–11,14,16] viz., sodium aluminate, aluminium isopropoxide and aluminium sulphate. Further, we have also varied the silicon-to-aluminium ratio so as to investigate the influence on the acidic sites and their catalytic activity for the chosen reaction.

2. Experimental

2.1. Starting materials

Sodium aluminate ($NaAlO_2$; EM Science; 32.9% Al), aluminium sulphate ($Al_2(SO_4)_3 \cdot 16H_2O$; SD'S; 98%) and aluminium isopropoxide ($Al(C_3H_7O)_3$; Aldrich; 99%) were used as the aluminium sources. Fumed silica (SiO_2; Aldrich; 99.8%) and cetyltrimethylammonium bromide ($C_{19}H_{42}NBr$; CTAB, Aldrich; 99%) were used as sources for silicon and surfactant, respectively. Tetramethylammonium hydroxide ($C_4H_{13}NO$; TMAOH, Aldrich; 25 wt.%) and sodium hydroxide (NaOH; Loba; 98%) were used as organic and alkali bases, respectively.

2.2. Synthesis of Na-AlMCM-41

The sodium form of the samples (Na-AlMCM-41) were prepared according to a procedure described elsewhere [10,30], having the gel (molar) composition of: $2SiO_2$:$0.27(CTA)_2O$:$0.26Na_2O$:$0.26(TMA)_2O$:xAl_2O_3:$120H_2O$ ($x = 0.033$, 0.0167 and 0.011). The gel (pH $\sim$ 11.5) was kept in a Teflon-lined stainless steel autoclave and heated in an air oven at 373 K for 24 h for crystallization. The solid product obtained was washed, filtered and dried overnight at 373 K. The as-synthesized samples were calcined at 823 K in nitrogen atmosphere for 3 h followed by heating in air for 9 h at a heating rate of 1 K min^{-1}. The samples synthesized with sodium aluminate (SA), aluminium sulphate (AS) and aluminium isopropoxide (AIP) are designated as SA-41, AS-41 and AIP-41, respectively.

2.3. Preparation of H-AlMCM-41

All the calcined (Na-AlMCM-41) samples, i.e., prepared with different aluminium sources were protonated (H-AlMCM-41), as per the procedure outlined previously by repeated ion-exchange using 1 M ammonium nitrate solution at 353 K for 6 h. The ammonium exchanged (NH_4-AlMCM-41) samples were recalcined at 823 K for 6 h air [30].

2.4. Preparation of Al_2O_3/MCM-41

Incipient wetness method was employed for the preparation of Al_2O_3/MCM-41 as per the procedure outlined elsewhere [34]. Prior to loading, the siliceous MCM-41 sample was activated at 393 K for 1 h. The activated sample (1 g) was then treated with aqueous aluminium sulphate solution (0.01 M). The latter was added drop wise and the slurry was stirred gently for 2–3 h. The resulting sample was repeatedly washed with distilled water, filtered and dried at room temperature followed by heating at 353 K for 6 h. The sample was then subjected to calcination in air at 823 K for 8 h, and the final sample is referred to as Al_2O_3/MCM-41.

2.5. Characterization

All the samples were systematically characterized using several analytical and spectroscopic techniques. The experimental details the various techniques are given below.

2.5.1. X-ray diffraction (XRD)

XRD patterns were recorded for all the samples in order to check the formation and structure of AlMCM-41. The diffraction patterns were recorded in the 2θ range of 1–10° using Rigaku miniflex X-ray diffractometer with nickel filtered CuKα radiation ($\lambda = 1.5418$ Å). The scan speed and step size were 0.5° min^{-1} and 0.01°, respectively.

2.5.2. Thermogravimetry-differential thermal analysis (TG-DTA)

Simultaneous TG-DTA measurements were carried out on a Shimazdu DT-30 thermal analysis system under nitrogen atmosphere with a flow rate of 40 ml min^{-1} using $\sim$ 15 mg of the sample. The samples were heated in the temperature range 300–1073 K with a heating rate of 10 K min^{-1}.

2.5.3. Inductively coupled plasma-atomic emission spectroscopic (ICP-AES)

The elemental analysis of the various AlMCM-41 samples was carried out by ICP-AES technique on a Labtam Plasma Lab 8440 equipment. The solutions for the analysis were prepared as per the following procedure. About 100 mg of calcined sample was taken in a platinum crucible and was dissolved in H_2SO_4/HF mixture to obtain a clear solution. The excess acid was neutralized with H_3BO_3 prior to analysis. It was then transferred into a standard volumetric flask. This solution was used for the ICP-AES analysis.

2.5.4. ^{27}Aluminium magic angle spinning-nuclear magnetic resonance (^{27}Al MAS-NMR)

The spectra of various AlMCM-41 samples were recorded on a Bruker avance DPX 300 spectrometer using a Doty scientific cross polarized-magic angle spinning (CP-MAS) probe with a frequency of 78.15 MHz. Forty-five pulses were used for all the measurements with repetition times 3 s and the data were obtained at a MAS speed of 5 kHz. Aqueous aluminium nitrate solution (1 M) was employed as reference for aluminium nuclei. The tetrahedral-to-octahedral ratio of aluminium was calculated based on relative integral intensity of the peaks, as per the procedure outlined elsewhere [8].

2.5.5. Fourier transform infra-red (FT-IR)

The spectra of the various AlMCM-41 samples were recorded on a Nicolet Impact 400 equipment with a 4 cm^{-1} resolution and 128 scans in the mid IR region (400–4000 cm^{-1}) employing KBr pellet technique. About 100 mg of dry KBr was mixed with a little amount (10 mg) of the sample and thoroughly mixed by grinding for homogenization and dried using IR lamp. The fine powder was then pressed into a transparent, thin pellet at 5 tons cm^{-2}. These pellets were used for the IR spectral measurements.

2.5.6. Nitrogen sorption isotherms

N_2 adsorption–desorption measurements were performed at 77 K using a Sorptomatric 1990 surface area analyzer. Prior to adsorption, the samples were evacuated at 623 K for 12 h. The specific surface area, A_{BET}, was determined from linear part of Brunauer–Emmett–Teller (BET) equation.

2.6. Acidity measurements

2.6.1. Pyridine FT-IR

The pyridine FT-IR spectrum for various samples were recorded using a Matson Cygnus-100 spectrophotometer as per the following procedure. About 80 mg H-AlMCM-41 was pressed into a self-supporting wafer of 13 mm diameter and was preactivated under vacuum (10^{-3} Torr) at 573 K for 24 h. The background spectrum was recorded first after cooling the sample to room temperature. The pyridine was then injected (5 μl) at room temperature, and allowed to saturate for 30 min. The sample was then degassed at a desired temperature and the spectrum was then recorded. About 300 scans were co-added for each plot. The difference spectrum was obtained finally by subtracting the background spectrum recorded previously.

2.6.2. Temperature programmed desorption of ammonia (NH_3-TPD)

The acidic behaviour of the catalysts was also followed by NH_3-TPD. About 200 mg of the protonated sample was placed in quartz reactor and was activated at 773 K in air for 6 h followed by 2 h in helium with a flow rate of 50 ml min^{-1}. The sample was maintained at 373 K for 4 h prior to its exposure to 15 pulses of ammonia vapour (500 μl each) followed by purging with helium for an hour. The desorption of ammonia was carried out by heating the reactor up to 823 K at a uniform rate of 10 K min^{-1}. The amount of ammonia desorbed was estimated with the aid of thermal conducting detector (TCD) signal as response factor for ammonia. The desorption peaks were deconvoluted by using Gaussian function with temperature as variant.

2.7. Reaction procedure

The *tertiary*-butylation of phenol was carried out using 750 mg of H-AlMCM-41 catalyst in a fixed-bed flow reactor. Prior to the reaction, the catalyst was activated at 773 K in a flow of air for 8 h followed by cooling to reaction temperature (448 K) in nitrogen atmosphere. After an hour, the reactant mixture, i.e., phenol and *tertiary*-butyl alcohol (*t*-BA), with a desired ratio and weight hour space velocity (WHSV) was fed into the reactor using a liquid injection pump (Sigmamotor) using nitrogen as the carrier gas. The effluents were condensed and collected at every 30 min interval. The products, viz., *p*-*t*-BP, *o*-*t*-BP and *2*,*4*-di-*t*-BP, were identified by gas chromatography (NUCON 5700) using a SE-30 column, while the *m*-*t*-BP was analyzed with AT-1000 column. Further, the products were confirmed using a combined gas chromatography–mass spectrometry (GC-MS; Hewlett Packered G1800A) with HP-5 capillary column.

3. Results and discussion

The XRD patterns of various AlMCM-41 samples prepared with different aluminium sources shows typical reflections of hexagonal unidimensional mesoporous MCM-41 structure [3,4,35]. Table 1 summarizes the average unit cell parameters (a_0) for various samples. As expected, the unit cell dimensions increase as the aluminium content increases owing to the larger ionic size of trivalent aluminium (0.53 Å) than tetravalent silicon (0.40 Å) [36]. It is also interesting to note from this table that the aluminium content remains nearly close to the starting (gel) composition. However, a slight decrease in Si/Al ratio is noticed as compared to the starting gel composition. This may be due to an incomplete condensation of silica, which remains as soluble silica during the synthesis [11,16]. The surface area of all the calcined AlMCM-41 samples was found to be in the range of 850–1030 m^2/g, supports the mesoporous nature of catalysts. The FT-IR spectra of AlMCM-41 (not reproduced here) shows a broad band in the region 3200–3800 cm^{-1} are assigned to surface hydroxyl groups. On

Table 1
XRD, ICP-AES and ^{27}Al MAS-NMR data of various AlMCM-41 samples

Sample code[a]	XRD (a_0, Å)[b]		ICP-AES (Si/Al ratio)		^{27}Al MAS-NMR tetrahedral-to-octahedral ratio[c]	
	As-synthesized	Calcined	Synthesis gel	Calcined	As-synthesized	Calcined
SA-(30)	52.77	50.28	30	28	100	97
SA-(60)	51.47	49.22	60	53	100	99
SA-(90)	49.68	46.55	90	85	100	98
AS-(30)	51.64	50.36	30	25	100	90
AS-(60)	49.29	48.36	60	53	100	88
AS-(90)	48.94	45.83	90	84	100	89
AIP-(30)	50.96	46.01	30	22	100	88
AIP-(60)	51.99	47.02	60	55	100	88
AIP-(90)	48.71	45.20	90	88	100	89

[a] The number in parenthesis designate the silicon-to-aluminium (molar ratio).
[b] Calculated based on hexagonal unit cell formula $1/d^2 = 4/3\ (h^2 + hk + k^2/\ a^2)$.
[c] Calculated from the integrated intensities of peaks due to tetrahedral and octahedral species.

the other hand, the bands at 2922 and 2845 cm^{-1} are characteristic of hydrocarbon moieties of the as-synthesized sample, which disappear upon calcination indicating the removal of template molecules from the pores. FT-IR spectra also show two main absorption bands around 1090 and 810 cm^{-1}, for both as-synthesized and calcined samples (*not produced here*), corresponding to antisymmetric stretching and symmetric stretching vibration of ≡Si—O—T≡, respectively, while the absorption band ~465 cm^{-1} corresponds to bending vibration of ≡T—O— (T = Si or Al). In addition, the weak bands at ~960 cm^{-1} are attributed to defect sites (≡Si—OH). Since both Si–O$^-$ and Al–O$^-$ stretching bands appear nearly in the same region (800–1100 cm^{-1}) and hence they cannot be clearly distinguished. However, a small shift toward the higher wavenumber could be noticed for AlMCM-41 as compared to siliceous MCM-41 as a result of the incorporation of Al for Si in the framework structure. All these features are typical characteristics of aluminosilicate of MCM-41 structure [37,38].

The TG of as-synthesized samples follows a three stage weight loss, in agreement with literature [9,37]. The first stage loss is due to desorption (around 5%) of water and/or adsorbed gas molecules (303–393 K). The second stage weight loss (around 40%) corresponding to oxidative degradation of the template molecules (393–643 K). The third stage weight loss around 5% corresponding to the condensation of silanol groups (673–823 K). This is well supported by the respective DTA transitions, viz., endothermic and exothermic transition. These results further support the mesoporous nature. On the other hand, the TG-DTA analysis of the calcined sample showed around 25% weight loss (323–373 K) with endothermic transition is due to adsorbed water molecules suggesting hydrophilic characteristics of the samples.

Fig. 1 depicts ^{27}Al MAS-NMR spectra of various as-synthesized samples. All the spectra show a

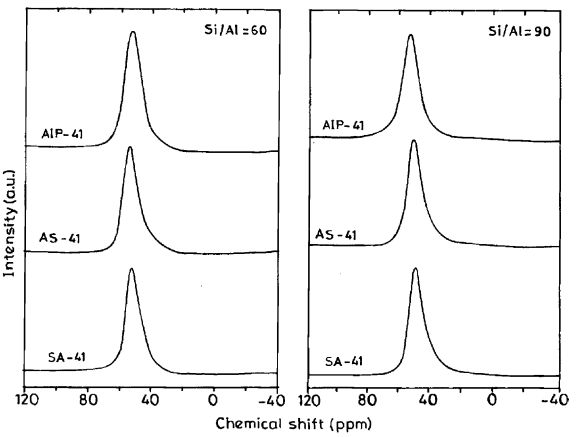

Fig. 1. ^{27}Al MAS-NMR spectra of as-synthesized Na-AlMCM-41 synthesized from different aluminium sources with various silicon-to-aluminium ratios.

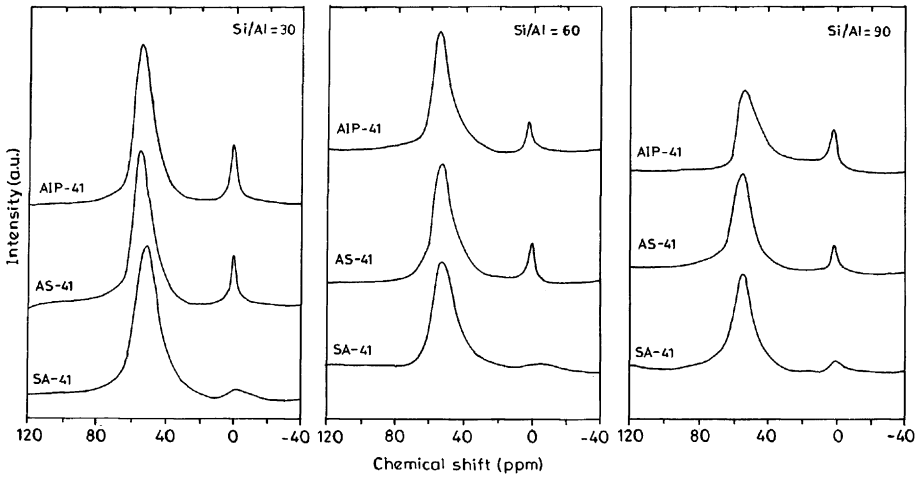

Fig. 2. ^{27}Al MAS-NMR spectra of calcined Na-AlMCM-41 synthesized from different aluminium sources with various silicon-to-aluminium ratios.

strong signal around +52 ppm corresponding to tetrahedral aluminium in the frame work position [8–10]. However, upon calcination the spectra (Fig. 2) show additional weak signal around 0 ppm that is a typical characteristics of aluminium in the octahedral coordination [9]. Furthermore, the main signals are broadened with the increase in aluminium content indicating a possible distortion of aluminium in the framework. On the other hand, the amount of octahedral aluminium in the non-framework strongly varies with the aluminium sources. As can be seen from Fig. 2 and Table 1 that among the three different aluminium sources used for the preparation of AlMCM-41, sodium aluminate retain a maximum aluminium in tetrahedral framework position even after calcination. In other words, the aluminium does not dislodge from the matrix during template removal. This could possibly be due to the fact that during aluminium incorporation in the tetrahedral silicate matrix, the trivalent aluminium may uniformly be distributed in the mesoporous framework structure of MCM-41 owing to the ease in the generation and incorporation of reactive monomeric $Al(OH)_4^-$ species [16,39]. On the other hand, the sample synthesized using aluminium isopropoxide and aluminium sulphate leads to a significant dislodgement of aluminium from the framework upon calcination. This observation is in good agreement with literature [9,14,16]. It is thus suggested that the use of low water soluble aluminium isopropoxide [8] and less reactive aluminium sulphate [11] as aluminium sources for the aluminium incorporation in the matrix may distribute aluminium unevenly which upon calcination easily dislodge the aluminium from the framework positions. As a result, octahedral aluminium is produced in these cases.

Fig. 3 shows the pyridine IR spectra of various H-AlMCM-41. All the samples show bands corresponding to hydrogen-bonded pyridine (1447 and 1599 cm^{-1}), Lewis acidic sites bound pyridine (1450 and 1623 cm^{-1}) and Brönsted acidic sites bound pyridine (1545 and 1640 cm^{-1}). An additional band appears 1490 cm^{-1} attributed to pyridine associated with both Brönsted and Lewis acidic sites [40–42]. It can be seen from figure that the increase in aluminium content lead to an increase in acidic sites, viz., Lewis and Brönsted acidic sites, which is in good agreement with Wang et al. [42]. Further, the amount of Lewis acidic sites increases in the order of sodium aluminate < aluminium sulphate $\leqslant$ aluminium isopropoxide, which is in good agreement with ^{27}Al MAS-NMR results (see Fig. 2 and Table 1). It is also interesting to note from Table 2 that the relative ratios of Brönsted-to-Lewis acidic sites further support the above conjuncture. Due to the overlapping

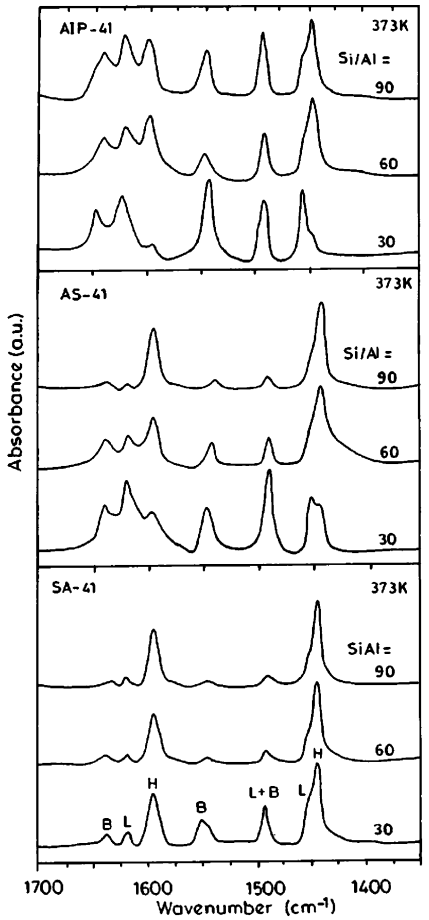

Fig. 3. Pyridine-FT-IR (desorption) spectra of H-AlMCM-41 synthesized with different aluminium sources with various silicon-to-aluminium ratio at 373 K.

Table 2
Pyridine FT-IR and NH_3-TPD data of H-AlMCM-41

Catalyst	Si/Al (molar ratio)	Pyridine FT-IR[a]	NH_3-TPD[b]
		B_{1640}/L_{1623}	$B_{(ii+iii)}/L_{(iv+v)}$
SA-41	90	0.98	3.55
	60	0.92	3.58
	30	0.76	2.47
AS-41	90	0.99	2.90
	60	0.89	2.71
	30	0.67	1.92
AlP-41	90	0.75	2.61
	60	0.74	2.40
	30	0.63	2.10

B—Brönsted acid site; L—Lewis acid site.
[a] Intensity ratios at 373 K.
[b] Area ratios.

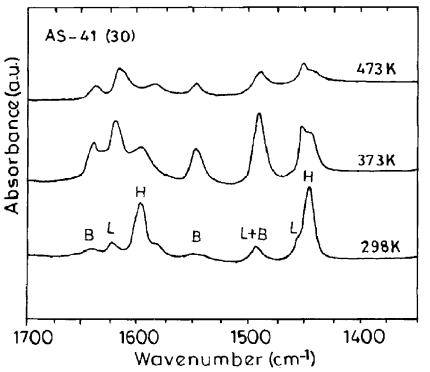

Fig. 4. Pyridine-FT-IR (desorption) spectra over H-AlMCM-41 at different temperatures.

hydrogen-bounded pyridine band (1447 cm^{-1}) and Lewis-bounded pyridine (1450 cm^{-1}), we express the Brönsted/Lewis ratio by the ratio of intensity of 1640/1623 cm^{-1}, which are well distinguish. Fig. 4 depicts pyridine FT-IR spectra of H-AlMCM-41 (AS-41) at different temperatures. It is clear from the figure that as the desorption temperature is increased from 298 to 373 K, the hydrogen bond bound pyridine band intensity decreases drastically, correspondingly both the Brönsted and Lewis acidic sites bound pyridine band intensity increases. Further, at higher temperature the Brönsted acidic sites bound intensity also decreases indicating the moderate acidic character. Fig. 5

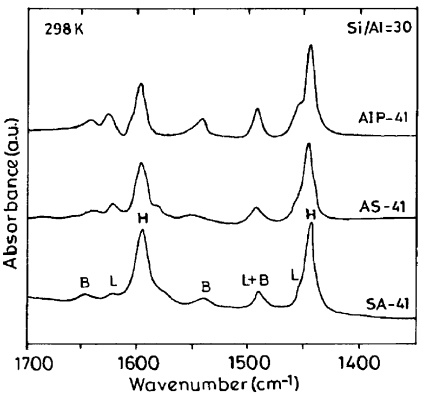

Fig. 5. Pyridine FT-IR (desorption) spectra over H-AlMCM-41 synthesized with different aluminium source at 298 K.

presents the pyridine FT-IR spectrum of AlMCM-41, having a silicon-to-aluminium ratio of 30, synthesized with different sources. It is clear from figure that the sample synthesized using sodium aluminate shows relatively low Lewis acid sites as compared to the samples prepared using aluminium sulphate and aluminium isopropoxide (see Table 2).

Fig. 6 depicts the NH_3-TPD traces of various H-AlMCM-41. The desorption peaks were deconvoluted by using Gaussion function with temperature as variant [43,44]. The first peak, around 420–440 K, referred to as type (i) is attributed to surface hydroxyl groups (weak acid sites), whereas the two other peaks, viz., type (ii) and (iii), in the range 450–480 and 540–600 K originate from moderate and strong structural (Brönsted) acid sites, respectively owing to the presence of trivalent aluminium in two different framework positions [31]. The broad and weak peak around 650–700 K, designated as type (iv), is attributed to weak Lewis acid sites, which may arise from tricoordinated aluminium in the framework. Evidence for such type of tricoordinated aluminium species has been deduced from ^{27}Al MAS-NMR studies for the water or acetylacetonate adsorbed AlMCM-41 surface [45]. A further increase in temperature (>750 K) resulted in a distinct peak, designated as type (v), corresponding to strong Lewis acid sites. This could be attributed to the possible dislodgement of aluminium from the framework structure leading to the formation of aluminium oxide clusters. It can also be noticed from these TPD traces that the amount of acid sites increases with increase in aluminium content. In addition, the relative area under the type (ii) and (iii) acid sites increases with increase in aluminium content. Further, at higher aluminium content (lower Si/Al ratio) noticeable increase in type (iv) acid sites is seen due to the formation of structural Lewis acid sites. This is consistent with ^{27}Al MAS-NMR and pyridine IR studies, as well

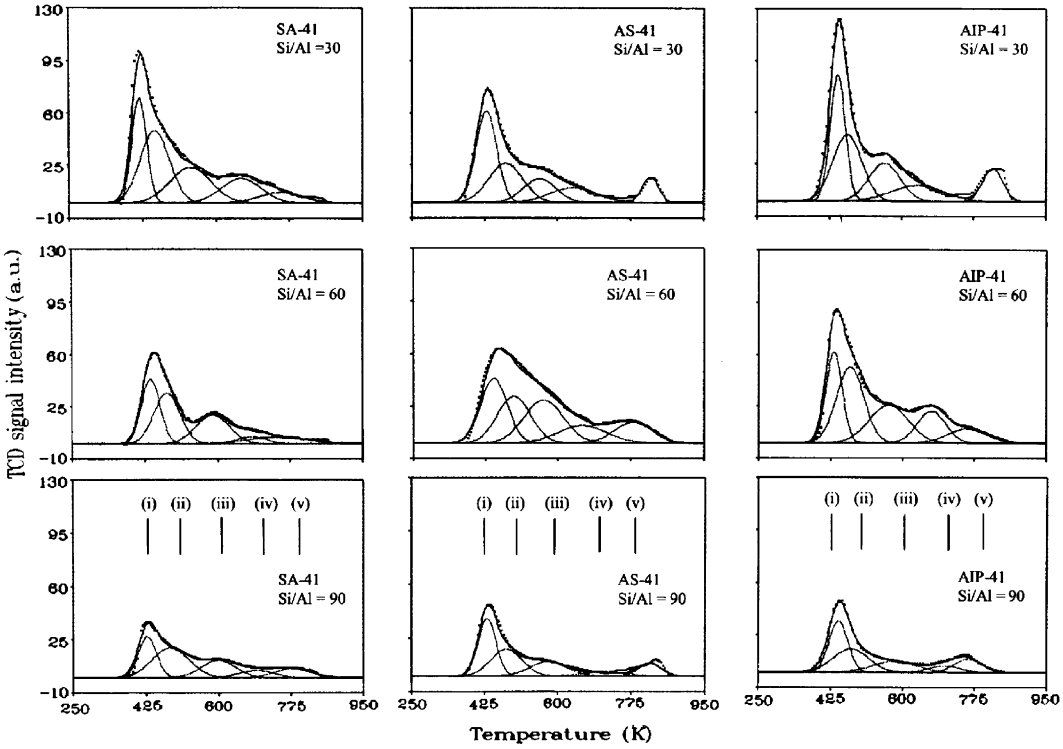

Fig. 6. NH_3-TPD of H-AlMCM-41 with various silicon-to-aluminium ratios.

Table 3
Alkylation of phenol with tertiary-butylalcohol over H-AlMCM-41 catalyst[a]

Catalyst	SA-41			AS-41			AIP-41			MCM-41	Al_2O_3/MCM-41
Si/Al ratio	30	60	90	30	60	90	30	60	90	$\propto$	60
Conversion (wt.%)	13.4	27.4	14.4	8.6	28.5	16.6	12.1	24.5	19.9	1.0	4.7
Selectivity (%)											
o-*t*-BP	5.2	3.3	0.7	5.8	5.6	5.4	7.0	8.2	6.0	43.1	10.6
m-*t*-BP	25.4	2.6	–	23.3	4.6	5.4	18.6	13.9	–	–	–
p-*t*-BP	68.7	91.5	99.3	70.9	88.4	86.8	74.4	76.3	93.5	46.9	89.4
2,4-di-*t*-BP	0.7	2.6	–	–	1.4	2.4	–	1.6	0.5	–	–

[a] Reaction conditions: Temperature = 448 K; W.H.S.V. = 4.8 h^{-1}; Time on stream = 1.5 h.

as the TPD peak assignment by Kosslick et al. [12].

Table 3 summarizes the results of tertiary butylation reaction of phenol over various H-Al-MCM-41. It can be seen from this table that the conversion and selectivity depends highly on the total amount of the type (ii) and (iii) acid sites. The conversion increases with increase in aluminium content, i.e., on going from 90 to 60 ratio, due to an increase in total amount of acid sites as well as presence of relatively more amount of type (ii) and (iii) acid sites (see Fig. 6), as moderate-to-strong acid sites favour the reaction [30,43,46]. However, a further increase in aluminium content, i.e., from 60 to 30 ratio, a considerable decrease in conversion was noticed. The observed lower conversion could be attributed to a possible dealkylation of *p*-*t*-BP owing to presence of more Lewis acidic sites (Table 2). These results are good agreement with pyridine FT-IR studies (see Fig. 3). Furthermore, the selectivity of *p*-*t*-BP decreases with the increase

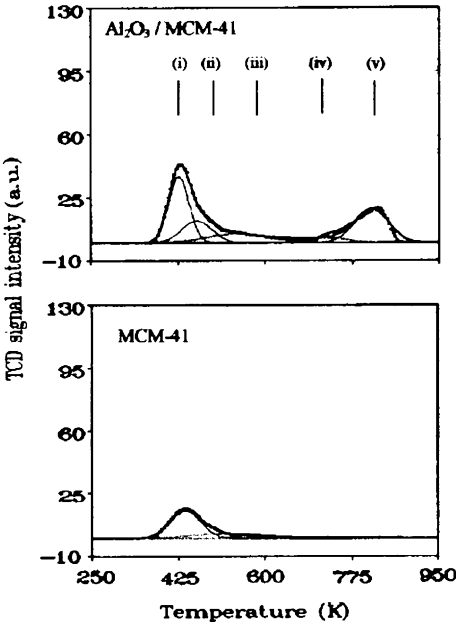

Fig. 7. NH_3-TPD of Al_2O_3/MCM-41 and MCM-41.

Table 4
Comparison of reaction data over H-AlMCM-41 and other catalysts under optimum reaction conditions

Catalysts	H-AlMCM-41 [This work]	SAPO-11[a] [27]	Zeolite-β [28]	Zeolite-Y[a] [33]
Phenol: *t*-BA	2:1	2:1	4:1	2:1
WHSV (h^{-1})	4.8	2.0	2.0	2.4
Temperature (K)	448	448	448	443
Conversion (wt.%)	27.4	39.3	25.4	45.5
Selectivity (%)				
o-*t*-BP	3.3	10.4	3.3	12.6
m-*t*-BP	2.6	–	38.2	–
p-*t*-BP	91.5	80.2	58.1	62.6
2,4-di-*t*-BP	2.6	6.4	0.4	18.1

[a] Some aromatics and cracking products also observed.

of aluminium content in the samples due to isomerization of *p-t*-BP into *m-t*-BP owing to the presence of the type (iv) acid sites, which normally favour such type of secondary reactions [29,30,43]. It is however, noteworthy here that type (i) and (v) acid sites are not responsible for the catalytic activity. This was confirmed by reaction over both aluminium free MCM-41 and Al_2O_3 loaded MCM-41, where the former contains only type (i) acid sites while the latter posses mainly type (i) and (v) acid sites (Fig. 7), and therefore the low activity (see also Table 3).

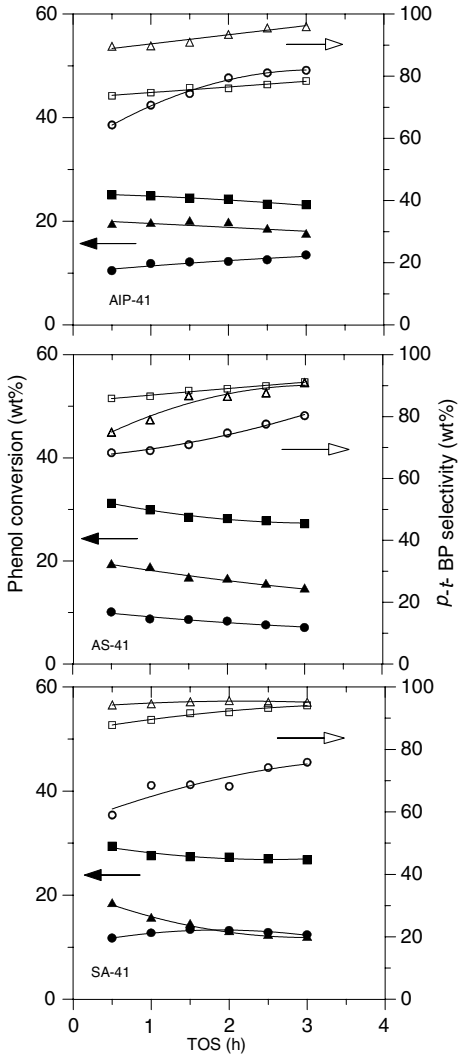

Fig. 8. Effect of time on stream on phenol conversion (filled symbols) and *p-t*-BP selectivity (open symbols) over various H-AlMCM-41 with silicon-to-aluminium ratio of 30 (●,○); 60 (■, □) and 90 (▲,△).

Table 4 presents a comparison of reaction data of H-AlMCM-41 with microporous molecular sieve-based catalysts such as SAPO-11 [27], zeolite-β [28] and zeolite-Y [33]. It is, however, clear from this table that among the various catalysts used for the chosen reaction, the former, i.e., H-AlMCM-41, shows much higher *p-t*-BP selectivity. Fig. 8 summarizes the effect of time on stream on H-AlMCM-41 synthesized using various aluminium sources as well as Si/Al ratios. It is clear from figure that for all the samples there is no appreciable change in conversion even after 3 h. However, in all cases, the catalyst showed slight deactivation with TOS. Further, the observed higher deactivation in the sample with Si/Al ratio of 90 is possibly be due to presence of relatively less type (ii) and (iii) acid sites. Further, in all the cases the *p-t*-BP selectivity increase with increase in TOS could be due to reduction of secondary reaction with reaction time.

4. Conclusion

In summary, it can be concluded from this study that among the various aluminium sources used, the use of sodium aluminate as aluminium source leads to maximum aluminium in the tetrahedral environment. In addition, the catalyst with a Si/Al ratio of 60 showed high activity for the chosen reaction. FT-IR pyridine adsorption and NH_3-TPD studies reveal that the catalysts contain various types of acid sites and that the moderate-to-strong acid sites, i.e., type (ii) and (iii) are responsible for the tertiary butylation reaction of phenol. Further, it can also be noticed that the presence of more type (ii) and (iii) acid site as well as the low ratio of type (ii)/(iii) acid sites led to higher phenol conversion.

Acknowledgements

This work was supported by the Board of Research in Nuclear Sciences (Department of Atomic Energy) under a contract no. 99/37/31/BRNS/

1049. The authors thank RSIC, IIT-Bombay for ICP-AES and GC-MS analysis.

References

[1] E.H. Knozinger, J. Weitkamp (Eds.), Handbook of Heterogeneous Catalysis, VCH, Weinheim, 1997, Vol. 5; J.H. Clark, D.J. Macquarrie, Org. Process Res. Develop. 1 (1997) 149.
[2] P.B. Venuto, P.S. Landis, Adv. Catal. 18 (1968) 259; P.B. Venuto, Micropor. Mater. 3 (1994) 297.
[3] C.T. Kresge, M.E. Leonowicz, W.T. Roth, J.C. Vartuli, J.S. Beck, Nature 359 (1992) 710.
[4] J.S. Beck, J.C. Vartuli, W.J. Roth, M.E. Leonowicz, C.T. Kresge, K.D. Schmitt, C.T.-W. Chu, D.H. Olson, E.W. Sheppard, S.B. McCullen, J.B. Higgins, J.L. Schelnker, J. Am. Chem. Soc. 114 (1992) 10834.
[5] D.T. On, D.D. Giscard, C. Danuman, S. Kaliaguine, Appl. Catal. A 222 (2001) 299.
[6] J.Y. Ying, C.P. Mehnert, M.S. Wong, Angew. Chem. Int. Ed. 38 (1999) 56.
[7] A. Corma, Chem. Rev. 97 (1997) 273.
[8] M. Janicke, D. Kumar, G.D. Stucky, B.F. Chemlka, Stud. Surf. Sci. Catal. 84 (1994) 243.
[9] R.B. Borade, A. Clearfield, Catal. Lett. 31 (1995) 267.
[10] Z. Luan, C.F. Cheng, W. Zhou, J. Kilnowski, J. Phys. Chem. 99 (1995) 1018.
[11] K.M. Reddy, C. Song, Catal. Lett. 36 (1996) 103; K.M. Reddy, C. Song, Catal. Today 31 (1996) 137.
[12] H. Kosslick, H. Landmesser, R. Fricke, J. Chem. Soc., Faraday Trans. 93 (1997) 1849; H. Kosslick, G. Lischke, B. Parlitz, W. Storek, R. Fricke, Appl. Catal. A 184 (1999) 49.
[13] S.B. Pu, J.B. Kim, M. Seno, T. Inui, Micropor. Mater. 10 (1997) 25.
[14] M.L. Occelli, S. Biz, A. Auroux, G.J. Ray, Micropor. Mesopor. Mater. 26 (1998) 195.
[15] S. Biz, M.G. White, J. Phys. Chem. 103 (1999) 8432.
[16] S.K. Badamali, A. Sakthivel, P. Selvam, Catal. Today 63 (2000) 291.
[17] Y. Cesteros, G.L. Haller, Micropor. Mesopor. Mater. 43 (2001) 171.
[18] A.J. Kolka, J.P. Napolitano, G.G. Elike, J. Org. Chem. 21 (1956) 712.
[19] K. Kagami, Y. Takami, JP. Patent 75 (1975) 112–325.
[20] S. Namba, T. Yahima, Y. Itaba, H. Hara, Stud. Surf. Sci. Catal. 5 (1980) 105.
[21] E.M. Viorica, E.S.A. Meroiu, H. Justin, O. Maria, C. Eleonora, Rom. Patent 73 (1981) 994.
[22] R.F. Parton, J.M. Jacobs, D.R. Huybrechts, P.A. Jacobs, Stud. Surf. Sci. Catal. 46 (1988) 163.
[23] A. Corma, H. Garcia, J. Primo, J. Chem. Res. (S) (1988) 40.
[24] C.D. Chang, S.D. Hellring, US Patent 5 (1994) 288–927.
[25] M. Yamamoto, A. Akyama, JP. Patent 6 (1994) 122–639.
[26] A.U.B. Queiroz, L.T. Aikawa, French Patent 2 (1994) 694000.
[27] S. Subramanian, A. Mitra, C.V.V. Satyanarayana, D.K. Chakrabarty, Appl. Catal. A 159 (1997) 229.
[28] A. Mitra, Ph.D. Thesis I.I.T-Bombay, 1997, p. 55.
[29] K. Zhang, C. Hunag, H. Zhang, S. Xiang, S. Liu, D. Xu, H. Li, Appl. Catal. A 106 (1998) 89; K. Zhang, H. Zhang, G. Xu, S. Xiang, D. Xu, S. Liu, H. Li, Appl. Catal. A 207 (2001) 183.
[30] A. Sakthivel, S.K. Badamali, P. Selvam, Micropor. Mesopor. Mater. 39 (2000) 457.
[31] S.K. Badamali, A. Sakthivel, P. Selvam, Catal. Lett. 65 (2000) 153.
[32] A. Sakthivel, N. Saritha, P. Selvam, Catal. Lett. 72 (2001) 225.
[33] R. Anand, R. Maheswari, K.U. Gore, B.B. Tope, J. Mol. Catal. A 193 (2003) 251.
[34] S.E. Dapurkar, S.K. Badamali, P. Selvam, Catal. Today 68 (2001) 63.
[35] P. Selvam, S.K. Bhatia, C.G. Sonwane, Ind. Eng. Chem. Res. 40 (2001) 3237.
[36] R.D. Shannon, C.T. Prewitt, Acta. Crystallogr. B 25 (1969) 925.
[37] C.Y. Chen, H-X. Li, M.E. Davis, Micropor. Mater. 2 (1993) 17.
[38] K. Vidya, S.E. Dapurkar, P. Selvam, S.K. Badamali, D. Kumar, N.M. Gupta, J. Mol. Catal. A 181 (2002) 91, 191 (2003) 149.
[39] M. Hartmann, C. Bischot, Stud. Surf. Sci. Catal. 117 (1998) 249.
[40] R. Mokaya, W. Jones, Z. Luan, M.D. Alba, J. Kilnowski, Catal. Lett. 37 (1996) 113.
[41] A. Corma, V. Fornes, M.T. Navarro, J. Perez-Pariente, J. Catal. 148 (1994) 569.
[42] J. Wang, L. Huang, H. Chen, Q. Li, Catal. Lett. 55 (1998) 157.
[43] S.K. Badamali, A. Sakthivel, P. Selvam, in: D.D. Do (Ed.), Adsorption Science and Technology, World Scientific, Singapore, 2000, p. 553.
[44] H.G. Karge, V. Dondur, J. Weitkamp, J. Phys. Chem. 95 (1991) 283.
[45] D.T. On, S.M.J. Zaidi, S. Kaliguine, Micropor. Mesopor. Mater. 22 (1998) 211.
[46] N.S. Chang, C.C. Chen, S.J. Chu, P.Y. Chen, T.K. Chuang, Stud. Surf. Sci. Catal. 46 (1989) 223.